Characterization of a fiber-optic displacement sensor for measurements in high-intensity focused ultrasound fields

Julian Haller,[a] Volker Wilkens, Klaus-Vitold Jenderka, and Christian Koch
Physikalisch-Technische Bundesanstalt, Bundesallee 100, 38116 Braunschweig, Germany

(Received 30 November 2010; revised 23 March 2011; accepted 30 March 2011)

A fiber-optic sensor is presented that is capable of measuring the particle displacement in high-intensity focused ultrasound (HIFU) fields. For this probe, a secondary calibration was performed, and the resulting complex frequency response is discussed. As a first practical application, the setup was used to measure the pressure in the field of a weakly focusing ultrasound transducer. The result is compared with that of a membrane hydrophone measurement. The feasibility of measurements in HIFU fields is demonstrated by means of measurements of the spatial distribution of the peak particle velocity within the focus of a HIFU transducer and of the dependence of the peak values on the acoustical power level. © *2011 Acoustical Society of America*. [DOI: 10.1121/1.3583538]

PACS number(s): 43.35.Yb, 43.35.Sx, 43.58.Fm [TDM] Pages: 3676–3681

I. INTRODUCTION

The incidence of high-intensity focused ultrasound (HIFU) as a noninvasive therapy technique for the treatment of tumors has been continuously growing in the past years.[1–5] Besides the treatment of prostate cancer and uterine myomas, other HIFU applications such as brain surgery,[6] heart surgery,[7] local drug delivery,[8] and pain palliation[9,10] as well as the treatment of other cancer types[11–13] are currently either in the research stage or already in the trial stage. The principle of all of these applications is to focus a large amount of acoustical energy into a small volume, where tissue heating, due to the sound absorption, and cavitation cause the respective desired effect, for example, the necrosis of tumor tissue. Although either the necrosis of tissue or the temperature elevation can be monitored with magnetic resonance imaging (MRI)[14] or B-mode ultrasound imaging[15] during the treatment, a very precise knowledge of the spatial and temporal distribution of the ultrasound field is of extremely high importance. Particularly, these data are needed as an input for the planning of a treatment with high therapeutic effect along with a minimal risk of undesired side effects.

Because in the focal region of HIFU fields acoustical intensities up to 20 000 W/cm^2 and heating rates up to 30 °C/s can occur,[5,16] sensors for the characterization of HIFU fields have to be very robust. Furthermore, for measurements with appropriate spatial and temporal resolution, sensors should both be small in dimension and have a fast response time. Conventional hydrophones, such as membrane hydrophones or needle hydrophones, usually do not withstand the high intensities in HIFU fields at levels that are required for clinical treatments. Hence several attempts have been made to develop piezoelectric sensors especially for HIFU fields.[17,18] A somewhat different but very promising attempt is to use fiber-optic hydrophones[19] for this purpose because they are small (typical diameter: 125 μm) and have already proved their high durability, for example, in shock wave measurements.[20–23] Several different types of fiber-optic probes have been developed for the measurement of ultrasound.[20–30] Two of them have recently been successfully applied to high-intensity ultrasound fields.

One sensor type consists of a perpendicularly cleaved fiber end face where a light beam is reflected.[20,21,28] As the refractive index of the surrounding medium and thus the reflectivity at the interface between the fiber and the medium changes with pressure, the reflected part of the light depends on the acoustic pressure of an incoming ultrasound wave. The other type of sensor is more complicated in production as several layers of different materials have to be applied onto the fiber tip, where they act as a microinterferometer, the reflectivity of which also depends on the acoustic pressure.[29–31] Whereas the first type has the advantage of having a very simple sensor design, which can be rebuilt quickly and cost-effectively when a sensor is destroyed, the second type usually shows higher signal-to-noise ratios.

Typically, hydrophones measure the pressure p in an ultrasound field and if the intensity I

$$I(t) = p(t) \cdot v(t) = p(t) \cdot \frac{\partial \xi(t)}{\partial t} \tag{1}$$

(v: particle velocity and ξ: particle displacement) is required, it is calculated as

$$I(t) = \frac{(p(t))^2}{\rho \cdot c_s} \tag{2}$$

(ρ: density and c_s: sound velocity for water) with implicitly using the equation

$$p(t) = \rho \cdot c_s \cdot \frac{\partial \xi}{\partial t}. \tag{3}$$

In general, Eq. (3), and thus Eq. (2), is only valid in a plane wave and therefore is inappropriate in many applications.

[a]Author to whom correspondence should be addressed. Electronic mail: julian.haller@ptb.de

 0001-4966/2011/129(6)/3676/6/$30.00

The common practice to use Eq. (2) for calculating the intensity is thus debatable because the validity of Eq. (3) in HIFU fields might be limited. In addition, the influence of nonlinear effects on intensity distributions is still under discussion.[32] Hence a measurement device for determining acoustic intensity in HIFU fields would be beneficial. As a first step, a fiber-optic measurement system is presented that detects the particle velocity in the sound field instead of pressure as in most other devices. The sensor is of simple construction and is interrogated by a heterodyne interferometer.

Strictly speaking, ξ, v, and thus also I have a certain direction and hence should be vectorially. However, it is common practice to consider only the axial components of the sound fields. Nevertheless, a more detailed investigation of this topic would be desirable especially for HIFU fields.

For any sensor with a non-constant frequency response, a signal with broad frequency bandwidth can be reliably derived from the measured voltages via deconvolution with the broadband complex frequency response of the sensor. HIFU waves are known to comprise several harmonics of the fundamental frequency, and, hence, a calibration of the frequency response has been performed for one sensor. Because a direct calibration of the particle velocity frequency response $M_v(f) = U(f)/v(f)$ is not possible, a calibration of the pressure frequency response $M_p(f) = U(f)/p(f)$ was performed instead.[33] However, Eq. (3) may be used in the sound field of the calibration, and thus the particle velocity frequency response can be easily calculated.

II. SETUP

For the present work, a batch of 12 sensors was manufactured from standard optical fiber pieces (single mode, 600 nm cut-off wavelength, 125 μm diameter, 250 μm coating), which were perpendicularly cleaved to get planar end faces. As a reflective coating, a 200 nm titanium layer was sputtered onto these end faces. Except for some changes to improve the optical performance, the optical setup is the same as the heterodyne interferometric configuration, which is described in more detail in Ref. 26 and is described only briefly here.

A laser diode with a frequency noise reducing external cavity (TUI Optics, Munich, Germany, Model DL 100, wavelength $\lambda_0 = 682$ nm, power $P_0 \leq 50$ mW) is utilized as a light source. Using an acousto-optic modulator (AOM) with $f_{\mathrm{AOM}} = 80$ MHz, the beam is split into a measurement beam with the original laser frequency $\nu_0 = c_0/\lambda_0$ ($c_0 = 3 \cdot 10^8$ m/s, speed of light) and a reference beam with a frequency that is shifted by the driving frequency of the AOM: $\nu_{\mathrm{ref}} = \nu_0 + f_{\mathrm{AOM}}$. The measurement beam is coupled into a fiber that has the reflecting sensor spliced to its end. When an ultrasound signal is applied to the sensor tip, the movement of the sensor tip will cause a change in the optical length δl in the measurement beam. This change is related to the particle displacement ξ of the sound wave in water via a transfer function $T(f)$:

$$\delta l = T \cdot \xi. \tag{4}$$

If the ideal transition of a plane wave from water to glas is considered, the ratio of the amplitudes of the particle velocities should be $T = \xi_{\mathrm{glas}}/\xi_{\mathrm{water}} = 2 \cdot Z_{\mathrm{water}}/(Z_{\mathrm{glas}} + Z_{\mathrm{water}})$, which yields roughly 0.2, when the acoustical impedances $Z_{\mathrm{water}} = 1.5 \cdot 10^6$ N·s·m^{-3} and $Z_{\mathrm{glas}} = 12 \cdot 10^6$ N·s·m^{-3} are used. However, $T(f)$ also comprises several diffraction and resonance effects and thus it is frequency-dependent.[22]

Due to the change in the optical path length, the acoustical signal is transferred into a phase modulation of the reflected measurement beam. The modulated light in the measurement beam interferes with the light of the reference beam at a beam splitter and is fed to a photodetector. Due to the photodetection process, a rf-voltage signal with frequency f_{AOM} is generated that carries the optical phase change as an electrical phase modulation. For this voltage signal, an instantaneous frequency f_{rf} can be defined as

$$f_{\mathrm{rf}}(t) = 2\pi f_{\mathrm{AOM}} + 2\pi \frac{2\nu_0 n}{c_0} \frac{\partial(\delta l)}{\partial t}, \tag{5}$$

where n is the refractive index of the fiber. Thus the output signal of the photo diode is

$$U_{\mathrm{out,PD}}(t) \propto \exp[i \cdot f_{\mathrm{rf}}(t) \cdot t]. \tag{6}$$

In a delay line discriminator (see Fig. 1) with delay time τ, this frequency modulation is demodulated into an amplitude modulation and an output signal $U_{\mathrm{out,D}}$ is generated with

$$U_{\mathrm{out,D}}(t) = D \cdot \frac{2 \cdot \nu_0 \cdot n}{c_0} \cdot \frac{\partial(\delta l)}{\partial t}. \tag{7}$$

Here D is the slope of the discriminator, which describes the ratio between the voltage output and the frequency deviation from the carrier frequency f_{AOM}. D can be easily determined by applying a well-known frequency deviation generated by a ring phase modulator in the measuring arm of the interferometer and measuring the corresponding voltage output of the discriminator. Using Eq. (4), Eq. (7) provides a simple relationship between the output voltage and the particle velocity v:

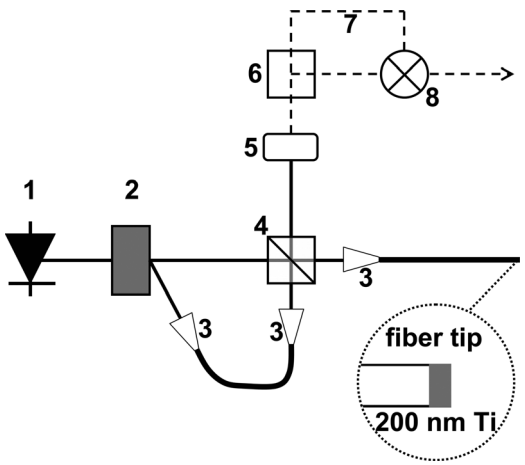

FIG. 1. Heterodyne interferometric setup for the displacement sensor. 1, laser diode; 2, AOM; 3, fiber coupler; 4, beam splitter; 5, photo diode; 6, 50:50 splitter; 7, delay line; 8, mixer. The discriminator consists of parts 6-8. A ring phase modulator in the measuring arm and polarization controllers in both arms are not depicted.

$$U_{\mathrm{out,D}}(t) = D \cdot \frac{2 \cdot v_0 \cdot n \cdot T}{c_0} \cdot \frac{\partial \xi}{\partial t} = D \cdot \frac{2 \cdot v_0 \cdot n \cdot T}{c_0} \cdot v. \qquad (8)$$

It should be noted that Eq. (8) is only valid as a good approximation as long as the discriminator is used in its linear range for the whole considered spectral bandwidth. Particularly, for a fixed discriminator delay time τ, a maximum detectable frequency $f_{\max} \approx \tau^{-1}$ can be found above which frequencies will not be demodulated linearly.[26]

III. CHARACTERISTICS

Despite that there have been some attempts made to derive the transfer function of fiber-optic sensors from calculations or simulations,[27,30] it seems to be essential for a correct analysis of the measurements to obtain the values of the amplitude as well as the phase of the transfer function for the individual measurement setup. Because no possibility to calibrate the particle velocity frequency response was available, a secondary calibration of the complex pressure frequency response $M_p(f) = U(f)/p(f)$ of the present setup was performed instead; this was in compliance with an established calibration procedure.[33] The particle velocity frequency response is then calculated as

$$M_v(f) = \rho \cdot c_s \cdot M_p(f) \qquad (9)$$

and the transfer function as

$$T(f) = \frac{\rho \cdot c_s \cdot c_0}{2 \cdot D \cdot v_0 \cdot n} \cdot M_p(f). \qquad (10)$$

This modus operandi is supposed to be correct here because a weakly focusing transducer is used within the calibration procedure and measurements are performed on the beam axis and at focal distance. The fact that the calibration used here yielded the same results as a time-delay spectrometry calibration, where only sound fields without nonlinearities are applied, for a similar displacement sensor,[22,23] supports this assumption.

In Fig. 2, the result of the calibration procedure is shown for frequencies up to 100 MHz. The amplitude shows a frequency behavior that is representative for this type of fiber-optic hydrophone because it has been observed during the calibrations for similar setups.[22,23,27,30,34] At 23 MHz, a resonance peak occurs that has been found to be due to a fiber end vibrational mode.[30] Another remarkable characteristic of the amplitude behavior obtained is an unexpectedly strong dip at 32 MHz. Although the deconvolution of measured signals should, in principal, compensate for any strong changes in the frequency response, it should be noted that such a strong dip might lead to a loss of information for that particular frequency region, leading to artifacts in the final time-dependent waveform. The strong peak at 80 MHz is due to cross talk by the carrier frequency. The phase behavior is quite similar to the one that was calculated under the assumption of minimum phase behavior.[23] Especially for frequencies below 20 MHz, it only differs by a linear factor, which simply results in a shift in the time domain. One major advantage of fiber-optic hydrophones is the fact that the geometrical dimensions of different tips of a batch are nearly the same due to the small tolerances in the fiber production. Typically, the diameter of the cladding should not vary by more than 1 μm and the excentricity between core and cladding by not more than 0.5 μm according to the manufacturer. This allows application of the calibration of the transfer function $T(f)$ that has been obtained for one single fiber tip to any other fiber tip of the same batch instead of calibrating every probe on its own. Any other effects that might go along with changing the sensor, as, for example, different absolute light intensities due to different splice losses, are presumed to be frequency-independent and thus are accounted for by the determination of the discriminator slope D before each measurement.

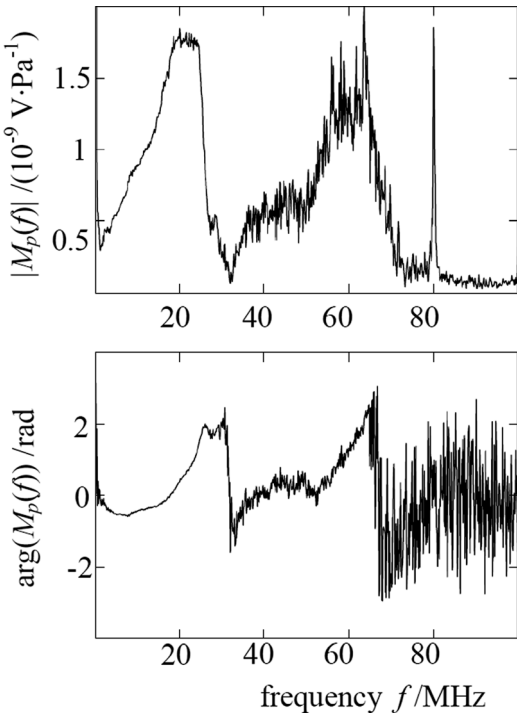

FIG. 2. Amplitude (top) and phase (bottom) of the pressure frequency response of the fiber-optic displacement sensor as derived from the secondary calibration procedure.

Another important characteristic of an ultrasound measuring device is the typical noise behavior. For the present setup, the signal-to-noise ratio for a measurement strongly depends on the discriminator delay line used. For the calibration, a delay line with $l = 0.6$ m ($D = 0.8$ mV/MHz) was used that exhibits a minimum detectable pressure (signal-to-noise ratio of 1 for a measurement) of 700 kPa at 100 MHz bandwidth and 200 kPa at 20 MHz bandwidth. [All minimum detectable pressure values mentioned were determined as follows: 64 voltage measurements without any ultrasound signal were averaged and divided by $M_p(1\ \mathrm{MHz}) = 0.5 \cdot 10^{-9}$ V/Pa. Then the standard deviation of the resulting $p_{\mathrm{noise}}(t)$ was taken as the minimum detectable pressure.] If a longer delay line with, for example, $l = 10$ m ($D = 5$ mV/MHz), is used, the minimum detectable pressure decreases to about 20 kPa at 20 MHz bandwidth, but at the same time, only frequencies up to 20 MHz will be demodulated linearly. Thus it is necessary to find a compromise between a wider resolution

bandwidth using a shorter delay line and better noise properties for a longer delay line.

IV. COMPARISON WITH A MEMBRANE HYDROPHONE

As a first test of the present setup, measurements were performed in the ultrasound field of a weakly focusing broadband transducer (TS12 PB2-7 P50, Karl Deutsch GmbH, Hürth, Germany, frequency range: from 0.7 to 12 MHz, diameter: 12 mm, nominal focal length: 50 mm), which was stimulated with a short electrical pulse of $U = 460$ V. Because the peak pressure values in this field are quite small (<1 MPa) and the spectra of the waveforms show no significant components above 20 MHz, a longer discriminator delay line ($l = 10$ m) was used here. For comparison, the sound field was measured with a calibrated membrane hydrophone[35] (260 μm effective diameter, 9 μm foil thickness) as well.

Figure 3 shows that the measurement performed with the fiber-optic setup is in quite good agreement with the measurement performed with the membrane hydrophone. The deviations that exceed the typical calibration uncertainty of 15% for low signals can be explained by the bad signal-to-noise ratio of the fiber sensor measurement for such small pressure values.

V. MEASUREMENTS IN HIFU FIELDS

Measurements were performed in the field of a HIFU transducer (Sonic Concepts, Bothell, WA, USA, Model H-108MRA, active diameter, 60 mm; focal length, 50 mm; fundamental frequency, $f_0 = 2.45$ MHz; electroacoustic efficiency, $\eta = 0.545$). The ultrasound signals were generated with an arbitrary function generator Tektronix, Beaverton, OR, Model AFG3101 and amplified with a broadband amplifier (ENI A-300). For the measurements in HIFU fields, a short delay line with $l = 0.6$ m was used. The voltage waveforms were averaged 512 times and recorded with a digital oscilloscope (Tektronix DPO7104) at full bandwidth (500 MHz). The respective electric power level of each measurement was determined with a power reflection meter Rohde & Schwarz, Munich, Germany, Model NRT, sensor head NAP Z-8). To constrain heating effects and for technical reasons (see Sec. VI), the measurements were performed with a burst mode signal (on-time: $\tau_{on} = 20$ cycles $= 8.2$ μs, pulse repetition frequency: $PRF = 1$ kHz). The electrical power levels were measured for continuous waves with the same output voltage of the function generator before each measurement, and the acoustical power levels were calculated by multiplication with the electroacoustic efficiency η, which was measured before with a radiation force balance and found to be constant for the considered power levels. Thus power levels are given as acoustic continuous wave equivalents.

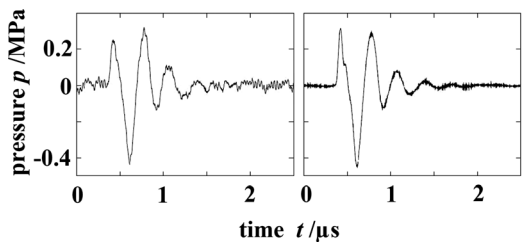

FIG. 3. Pressure waveform in the focus of a weakly focusing broadband transducer as measured with the fiber-optic setup (left, 64 times averaged) and a membrane hydrophone (right, single shot measurement).

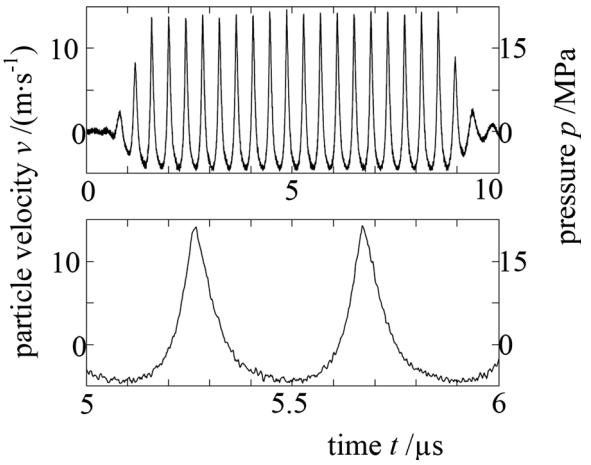

FIG. 4. Waveform $v(t)$ in the focus of a H-108MRA transducer at $P_{ac} = 25$ W as measured with the fiber-optic setup. The lower diagram is a magnified section of the upper one.

Figure 4 shows a typical particle velocity waveform as obtained from the measurements. The $v(t)$ waveforms were derived by transforming the measured transient voltages $U(t)$ into the frequency domain and dividing them by the complex frequency response (both low-pass filtered to 100 MHz with a Butterworth filter) and backtransformation into the time domain:

$$v(t) = \mathrm{FFT}^{-1}\left\{\frac{\mathrm{FFT}\{U(t)\}}{M_v(f)}\right\}. \tag{11}$$

FFT and FFT^{-1} denote a fast Fourier transformation and its inverse, respectively. Because the ultrasound particle velocity is a rather unusual value, the pressure values derived by using Eq. (3) are given on the right axis of Fig. 4. The same applies to the following figures.

In Fig. 5, a radial scan and an axial scan of the peak particle velocities through the focus of the transducer are

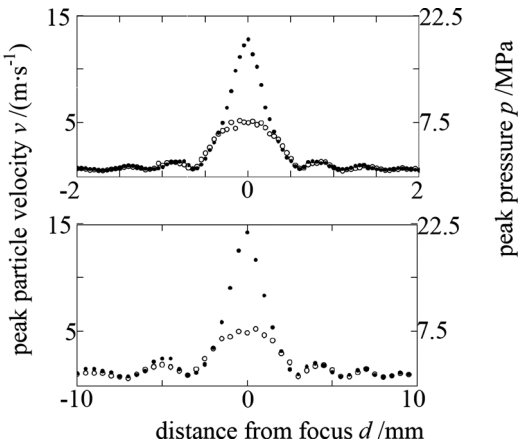

FIG. 5. Radial (top) and axial (bottom) scan of the peak particle velocity through the focus of a H-108MRA transducer at $P_{ac} = 25$ W as measured with the fiber-optic setup. Full symbols denote peak positive velocities and open symbols peak negative velocities.

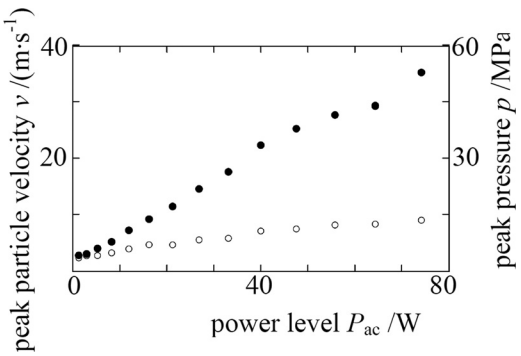

FIG. 6. Peak particle velocities in the focus of a H-108MRA transducer at different acoustical power levels as measured with the fiber-optic setup. Full symbols denote peak positive velocities and open symbols peak negative velocities.

shown. A spatial step size of 0.1 mm was chosen for the radial scans (0.5 mm for the axial scan); it approximately matches the sensor diameter.

To test the durability of the sensor as well, additional measurements were performed at increasing acoustical power levels. The resulting peak particle velocities are shown in Fig. 6. At the highest power level ($P_{ac} = 74$ W), cavitation occurred and removed the reflecting layer at the fiber tip. It should be noted that if Eq. (3) is assumed to be valid, the corresponding peak pressure values for this measurement would be as high as $p_c = 52$ MPa and $p_r = 13$ MPa; this means that the robustness of the fiber tip was quite satisfying.

VI. DISCUSSION

It has been shown that the presented fiber-optic displacement sensor is capable of measuring the particle velocity in HIFU fields with high spatial and temporal resolution and that it withstands considerable high pressure values.

The measurements demonstrate the need for a broadband calibration of the complex frequency response. In Fig. 7, the peak positive particle velocities are shown when derived from the measured voltages by simple scaling with the amplitude of the frequency response at the fundamental frequency f_0 or by deconvolution with the amplitude of the frequency

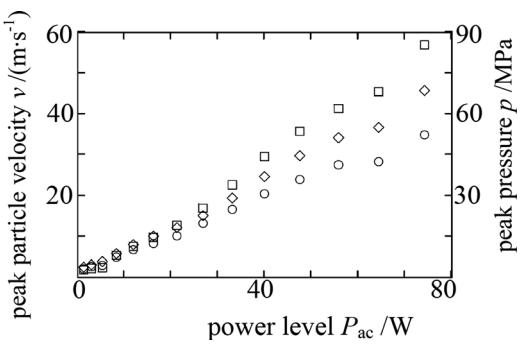

FIG. 7. Peak positive particle velocities in the focus of a H-108MRA transducer at different acoustical power levels as measured with the fiber-optic setup and analyzed via scaling with $|M(f_0)|$ (open square), deconvolution with $|M(f)|$ (open diamond), and deconvolution with complex $M(f)$ (open circle).

response alone or by deconvolution with the complex frequency response. It is obvious that the first two methods lead to an overestimation of the peak values of up to 50 or 30%, respectively.

The analysis of measurements in the time domain shows that delayed signals disturb the measurement results. Mechanical reflections appear within the fiber, especially at the beginning of the titanium coating and at points where mechanical stress is applied to the fiber, such as at any mounting points. Hence a stress-diminishing mounting was used here, where the fiber was glued into a carbon fiber tube. This kind of mounting additionally impedes possible evasive movements of the fiber that might appear due to the ultrasound radiation force. If an undisturbed measurement is required, existing reflections have to be excluded from measurements by time gating. Thus a measurement of continuous waves as used in therapeutic applications is not possible. However, this limitation arises not solely for fiber-optic probes, and for the spatial characterization of HIFU sound fields, the use of burst signals should be appropriate.

When higher acoustical power levels are to be investigated, cavitation unavoidably occurs in water. Although some of the investigated sensors withstood cavitation effects for a certain time, it was observed that enduring cavitation destroyed any sensor during a run of several hours. However, the presence of cavitation bubbles precludes reproducible measurements of the sound field anyway. It thus remains an open challenge to establish a way to suppress cavitation as far as possible to allow for field characterizations at very high ultrasound amplitudes.

VII. CONCLUSION

In this contribution, it was possible to show that the presented calibrated fiber-optic displacement sensor is capable of reproducibly measuring the particle velocity in HIFU fields. The sensor also proved to be satisfactorily robust because it withstood peak particle velocities of 35 m/s (positive, corresponding to $p_c \approx 52$ MPa)) and 10 m/s (negative, corresponding to $p_r \approx 13$ MPa). The small dimension of the sensor (125 μm diameter) allows tight focal regions to be measured with sufficient spatial resolution. Furthermore, the detection bandwidth, and thus the temporal resolution, can be adjusted by choosing an appropriate length of the discriminator delay line.

A calibration of the complex frequency response was accomplished, which allows for a correct analysis of the measured waveforms by means of deconvolution. For weak ultrasound fields, the uncertainty of the amplitude measurements is mainly determined by the uncertainty of the calibration (10-20 %, depending on frequency range[33]), whereas the uncertainties of measurements in HIFU fields cannot be seriously evaluated from the limited number of measurements carried out in this study. Besides the uncertainty evaluation, future work should investigate the validity of Eq. (3) at high intensity levels with the presented setup, on the one hand, and a pressure sensor, on the other hand. Furthermore, a combination of both types of sensor would allow for a measurement of instantaneous acoustical intensity.

ACKNOWLEDGMENTS

The present work was performed in the framework of the iMERA + project "JRP7 – External Beam Cancer Therapy," and financing by the European Union is gratefully acknowledged. We would also like to thank A. Shaw (NPL, London, UK), G. Durando (INRIM, Turine, Italy), and B. Karaböce (TUBITAK-UME, Istanbul, Turkey) for their fruitful collaboration.

[1]G. ter Haar and C. Coussios, "High intensity focused ultrasound: Past, present and future," Int. J. Hyperthermia **23**, 85–87 (2007).
[2]G. ter Haar, "Acoustic surgery," Phys. Today **54**, 29–34 (2001).
[3]A. Blana, B. Walter, S. Rogenhofer, and W. F. Wieland, "High-intensity focused ultrasound for the treatment of localized prostate cancer: 5-year experience," Urology **63**, 297–300 (2004).
[4]K. Rove, K. Sullivan, and E. Crawford, "High-intensity focused ultrasound: Ready for primetime," Urol. Clin. North Am. **37**, 27–35 (2010).
[5]G. ter Haar and C. Coussios, "High intensity focused ultrasound: Physical principles and devices," Int. J. Hyperthermia **23**, 89–104 (2007).
[6]N. McDannold, G. T. Clement, P. Black, F. Jolesz, and K. Hynynen, "Transcranial magnetic resonance imaging guided focused ultrasound surgery of brain tumors: Initial findings in 3 patients," Neurosurgery **66**, 323–332 (2010).
[7]S. Mitnovetski, A. Almeida, J. Goldstein, A. Pick, and J. Smith, "Epicardial high-intensity focused ultrasound cardiac ablation for surgical treatment of atrial fibrillation," Heart, Lung and Circ. **18**, 28–31 (2009).
[8]D. Chen and J. Wu, "An in vitro feasibility study of controlled drug release from encapsulated nanometer liposomes using high intensity focused ultrasound," Ultrasonics **50**, 744–749 (2010).
[9]B. Liberman, D. Gianfelice, Y. Inbar, A. Beck, T. Rabin, N. Shabshin, G. Chander, S. hengst, R. Pfeffer, A. Chechick, A. Hanannel, O. Dogadkin, and R. Catane, "Pain palliation in patients with bone metastases using MR-guided focused ultrasound surgery: A multicenter study", Ann. Surg. Oncol. **16**, 140–146 (2008).
[10]L. L. Xiong, J. H. Hwang, X. B. Huang, S. S. Yao, C. J. He, X. H. Ge, H. Y. Ge, and X. F. Wang, "Early clinical experience using high intensity focused ultrasound for palliation of inoperable pancreatic cancer," J. Pancreas **10**, 123–129 (2009).
[11]O. Esnault, B. Franc, and J. Chapelon, "Localized ablation of thyroid tissue by high-intensity focused ultrasound: Improvement of noninvasive tissue necrosis methods," Thyroid **19**, 1085–1091 (2009).
[12]K. Fischer, W. Gedroyc, and F. Jolesz, "Focused ultrasound as a local therapy for liver cancer," Cancer J. **16**, 118–124 (2010).
[13]F. Wu, Z. Wang, Y. Cao, W. Chen, J. Bai, J. Zou, and H. Zhu, "A randomised clinical trial of high-intensity focused ultrasound ablation for the treatment of patients with localised breast cancer," Br. J. Cancer **89**, 2227–2233 (2003).
[14]H. E. Cline, J. F. Schenck, K. Hynynen, R. D. Watkins, S. P. Souza, and F. A. Jolesz, "MR-guided focused ultrasound surgery," J. Comp. Assist. Tomogr. **16**, 956–965 (1992).
[15]G. Bouchoux, R. Berriet, C. Lafon, G. Fleury, D. Cathignol, J. Y. Chapelon, "Dual mode transducer for ultrasound monitored thermal therapy," Ultrasound Med. Biol. **34**, 607–616 (2008).
[16]I. Rivens, A. Shaw, J. Civale, and H. Morris, "Treatment monitoring and thermometry for therapeutic focused ultrasound," Int. J. Hyperthermia **23**, 121–139 (2007).
[17]C. I. Zanelli and S. M. Howard, "A robust hydrophone for HIFU metrology," in *Fifth International Symposium on Therapeutic Ultrasound*, edited by G. T. Clement, N. J. McDonald, and K. Hynynen (American Institute of Physics, New York, 2005), pp. 618–622.
[18]M. E. Schafer, J. Gessert, and W. Moore, "Development of a high intensity focused ultrasound (HIFU) hydrophone system," in *Fifth International Symposium on Therapeutic Ultrasound*, edited by G. T. Clement, N. J. McDonald, and K. Hynynen (American Institute of Physics, New York, 2005), pp. 609–613.
[19]G. Wild and S. Hinckley, "Acousto-ultrasonic optical fiber sensors: Overview and state-of-the-art," IEEE Sens. J. **8**, 1184–1193 (2008).
[20]J. Staudenraus and W. Eisenmenger, "Fiber-optic probe hydrophone for ultrasonic and shock-wave measurements in water," Ultrasonics **31**, 267–273 (1993).
[21]Z. Q. Wang, P. Lauxmann, C. Wurster, M. Köhler, B. Gompf, and W. Eisenmenger, "Impulse response of a fiber-optic probe hydrophone determined with shock waves in water," J. Appl. Phys. **85**, 2514–2516 (1999).
[22]C. Koch, G. Ludwig, and W. Molkenstruck, "Calibration of a fiber tip ultrasonic sensor up to 50 MHz and the application to shock wave measurement," Ultrasonics **36**, 721–725 (1998).
[23]C. Koch, W. Molkenstruck, and R. Reibold, "Shock-wave measurement using a calibrated interferometric fiber-tip sensor," Ultrasound Med. Biol. **23**, 1259–1266 (1997).
[24]B. Guan, Y. Tan, and H. Tam, "Dual polarization fiber grating laser hydrophone," Opt. Exp. **17**, 19544–19550 (2009).
[25]R. Chen, G. F. Durando, T. Butler, and R. A. Badcock, "A novel ultrasound fiber-optic sensor based on a fused-tapered optical fiber coupler," Meas. Sci. Technol. **15**, 1490–1495 (2004).
[26]C. Koch, "Measurement of ultrasonic pressure by heterodyne interferometry with a fiber-tip sensor," Appl. Opt. **38**, 2812–2819 (1999).
[27]C. Koch, G. Ludwig, and W. Molkenstruck, "Calibration of an interferometric fiber tip sensor for ultrasound detection," Ultrasonics **35**, 297–303 (1997).
[28]J. E. Parsons, C. A. Cain, and J. B. Fowlkes, "Cost-effective assembly of a basic fiber-optic hydrophone for measurement of high-amplitude therapeutic ultrasound fields," J. Acoust. Soc. Am. **119**, 1432–1440 (2006).
[29]V. Wilkens and C. Koch, "Fiber-optic multilayer hydrophone for ultrasonic measurement," Ultrasonics **37**, 45–49 (1999).
[30]W. Weise, V. Wilkens, and C. Koch, "Frequency response of fiber-optic multilayer hydrophones: experimental investigation and finite element simulation," IEEE Trans. Ultrason. Ferroelectr. Freq. Control **49**, 937–946 (2002).
[31]P. Morris, A. Hurrell, A. Shaw, E. Zhang, and P. Beard, "A Fabry-Pérot fiber-optic ultrasonic hydrophone for the simultaneous measurement of temperature and acoustic pressure," J. Acoust. Soc. Am. **125**, 3611–3622 (2009).
[32]A. Shaw and M. Hodnett, "Calibration and measurement issues for therapeutic ultrasound," Ultrasonics **48**, 234–252 (2008).
[33]V. Wilkens and C. Koch, "Amplitude and phase calibration of hydrophones up to 70 MHz using broadband pulse excitation and an optical reference hydrophone," J. Acoust. Soc. Am. **115**, 2892–2903 (2004).
[34]S. Umchid, R. Gopinath, K. Srinivasan, P. A. Lewin, A. S. Daryoush, L. Bansal, and M. El-Sherif, "Development of calibration techniques for ultrasonic hydrophone probes in the frequency range from 1 to 100 MHz," Ultrasonics **49**, 306–311 (2009).
[35]V. Wilkens and W. Molkenstruck, "Broadband PVDF membrane hydrophone for comparisons of hydrophone calibration methods up to 140 MHz," IEEE Trans. Ultrason. Ferroelectr. Freq. Control **54**, 1784–1791 (2007).